Electronic Supplementary Material (ESI) for Journal of Materials Chemistry C.
This journal is © The Royal Society of Chemistry 2023

New RM734-like Fluid Ferroelectrics Enabled through a Simplified Protecting Group Free Synthesis

Supplemental Information

Calum J. Gibb*, Richard. J. Mandle [1,2]

[1]School of Chemistry, University of Leeds, Leeds, UK, LS2 9JT
[2]School of Physics and Astronomy, University of Leeds, Leeds, UK, LS2 9JT

*c.j.gibb@leeds.ac.uk

Contents:

1 Experimental Methods

1.1. *Chemical Synthesis*

Chemicals were purchased from commercial suppliers (Fluorochem, Merck) and used as received. Solvents were purchased from Merck and used without further purification. Reactions were performed in standard laboratory glassware at ambient temperature and atmosphere and were monitored by TLC with an appropriate eluent and visualised with 254 nm light. Chromatographic purification was performed using a Combiflash NextGen 300+ System (Teledyne Isco) with a silica gel stationary phase and a hexane/ethyl acetate gradient as the mobile phase, with detection made in the 200-800 nm range. Chromatographed materials were subjected to re-crystallisation from an appropriate solvent system.

1.2 Chemical Characterisation Methods

The structures of intermediates and final products were determined using ^{1}H, $^{13}C\{^{1}H\}$, and, where appropriate, ^{19}F NMR spectroscopy. NMR was performed using a Bruker Avance III HDNMR spectrometer operating at 400 MHz, 100.5 MHz or 376.4 MHz (^{1}H, $^{13}C\{^{1}H\}$ and ^{19}F, respectively).

1.3 Mesophase Characterisation

Characterisation of the translational properties of compounds **1-11** were determined by differential scanning calorimetry (DSC) using a TA instruments Q200 heat flux calorimeter with a liquid nitrogen cooling system for temperature control. Samples were measured under a nitrogen atmosphere with 20 ℃ min^{-1} heating and cooling rates. The transition temperatures and enthalpy values reported are averages obtained for duplicate runs and normally extracted from heating traces. Phase identification by polarised optical microscopy (POM) was performed using a Leica DM 2700 P polarised optical microscope equipped with a Linkam TMS 92 heating stage. Samples were studied sandwiched between two untreated glass coverslips.

1.4 Simulation Setup and Analysis

Fully atomistic molecular dynamics (MD) simulations were performed in Gromacs 2019, [1–7]with parameters modelled using the General Amber Force Field (GAFF). [8] Atomic charges were determined using the RESP method [9] for geometry optimised at the B3LYP/6-31G(d) level of DFT [10,11] using the Gaussian G16 revision c01 software package. [12] Topologies were generated using AmberTools 16 [13,14] and converted into Gromacs readable format with Acpype. [15]

We initially constructed a low density lattice of 600 molecules of **10** with random positional and orientational order. Following energy minimization by the steepest decent method we performed short (5 ns) equilibration simulations in the NVE and NVT (T = 600 K) ensembles. We then performed a short 'compression' simulation (25 ns) at 600K with an isotropic barostat (P = 100 Bar) to compress the simulation to a liquid like density (~ 1.1 g cm^3). We then obtained a *polar* nematic configuration by applying a static electric field (1 V nm^{-1}) along the x-axis of the isotropic starting configuration for a total of 100 ns at 413 K and 1 Bar; this configuration was used as a starting point for subsequent simulations. Production MD simulations were performed without the biasing field and employed an anisotropic barostat (pressure of 1 Bar), at temperatures of 413 – 513 K in 10 K increments for a further 250 ns, unless otherwise noted.

Simulations employed periodic boundary conditions in xyz. Bonds lengths were constrained to their equilibrium values with the LINCS algorithm [16]. During production MD simulations the system pressure was maintained at 1 Bar using an isotropic Parrinello-Rahamn barostat. [17,18] Compressabilities in xyz dimensions were set to 4.5e-5, with the off-diagonal compressibilities were set to zero to ensure the simulation box remained rectangular. Simulation temperature was controlled with a Nosé–Hoover thermostat. [19,20] Long-range electrostatic interactions were calculated using the Particle Mesh Ewald method with a cut-off value of 1.2 nm. A van der Waals cut-off of 1.2 nm was used. MD trajectories were visualised using PyMOL 4.5. Q-tensor analysis was performed using MDTraj 1.9.8. [21]Cylindrical distribution functions (CDF) were computed using the *cylindr* code. [22] Simulation densities, dipole moments and volumes were obtained with the *gmx energy* program, with dipole and volume being used to compute spontaneous polarisation.

We calculate the second-rank orientational order parameter $<P_2>$ *via* the Q-tensor according to equation (1);

$$Q_{\alpha\beta} = \frac{1}{N}\sum_{m=1}^{N}\frac{3a_{m\alpha}a_{m\beta}-\delta_{\alpha\beta}}{2} \quad (1)$$

where N is the number of monomers, m is the monomer number within a given simulation, α and β represent the Cartesian x, y and z axes, delta is the Kronecker delta, *a* is a vector that describes the molecular long axis, which is computed for each monomer as the eigenvector associated with the smallest eigenvalue of the inertia tensor. The director at each frame was defined as the eigenvector associated with the largest eigenvalue of the ordering tensor. The order parameter <*P2*> corresponds to the largest eigenvalue of $Q_{\alpha\beta}$, and the biaxial order parameter <*B*> corresponds to the difference between the two smallest eigenvalues. The polar order parameter, <*P1*>, was calculated as the total dipole moment of the simulation box over the sum of the individual molecular dipoles. The polarization, *P*, was calculated from the total dipole of the box over the volume.

2 Supplemental Results

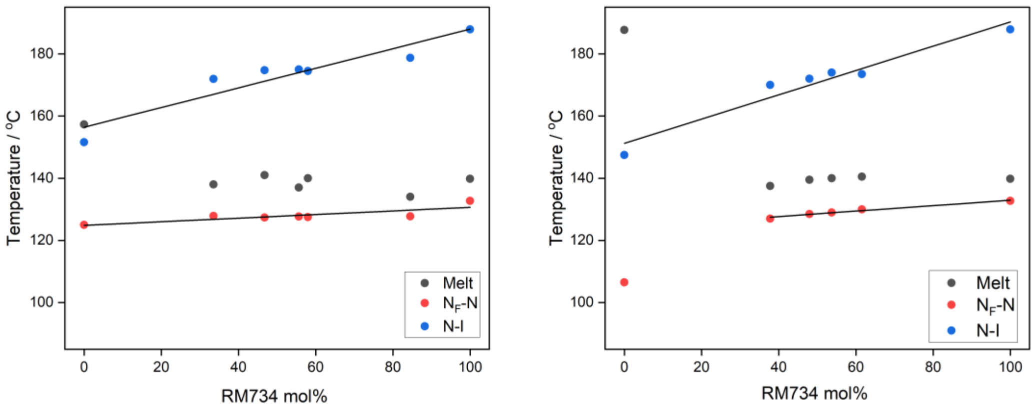

SIFig. 1 Phase diagram for the mixture of compound **3** (left) and compound **6** (right) with RM734.

3 Chemical synthesis

Compounds **1-11** were synthesised as outlined in SIScheme 1.

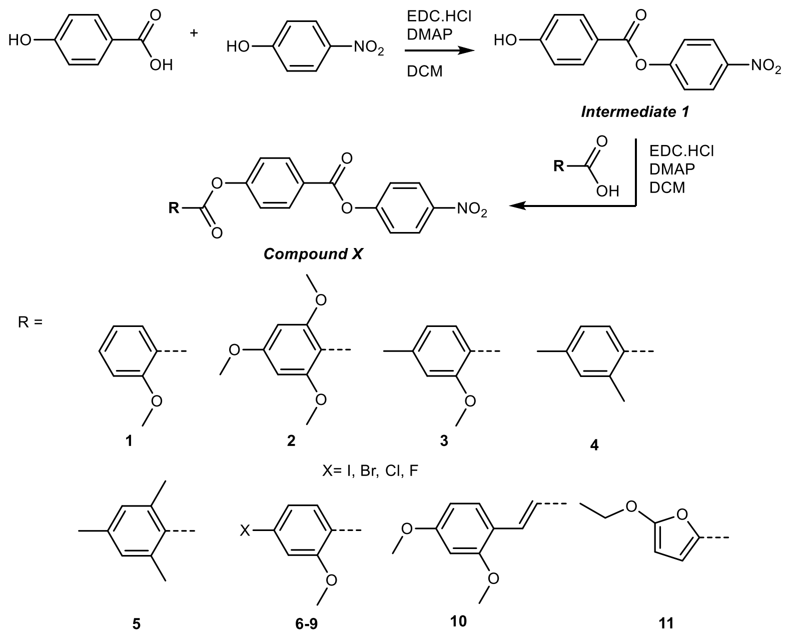

SIScheme 1: Synthesis of the RM734 derivatives, Compounds **1-11**.

2.1 Synthesis of 4-nitrophenyl 4-hydroxybenzoate (Intermediate 1)

A round bottomed flask was charged with 4-nitro phenol (10.0 g, 0.072 mol, 1 eqv.), 4-hydroxy benzoic acid (9.83 g, 0.072 mol, 1.0 eqv), EDC.HCl (20.7 g, 0. 108 mol, 1.5 eqv.) and DMAP (2 mol%). Dichloromethane was added (conc. ~ 0.1 M) and the suspension stirred until complete consumption of the phenol as judged by TLC. The volatiles were removed in vacuo and the crude material was subjected to flash chromatography over silica gel with a gradient of hexane/EtOAc. Intermediate **1** was then recrystallized from EtOH and dried under reduced pressure overnight to give the reported yield.

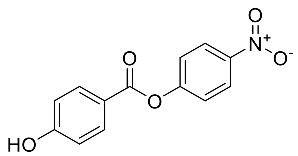

Intermediate **1**

White powder	10.8 g, 58 %
R_f (EtOAc): 0.68	
^{1}H NMR (400 MHz, DMSO-d6) (δ)	10.64 (s, 1H, Ar-O**H**), 8.33 (d, J = 8.9 Hz 2H, Ar-**H**), 8.01 (d, J = 8.1 Hz, 2H, Ar-**H**), 7.57 (d, J = 8.9 Hz, 2H, Ar-**H**), 6.94 (dd, J = 8.1, Hz, 2H, Ar-**H**).
^{13}C{^{1}H} NMR (101 MHz, DMSO-d6) (δ)	164.10, 163.57, 156.26, 145.40, 132.99, 126.63, 123.80, 119.03, 116.18.

2.2 Synthesis of Compounds 1-11

A round bottomed flask was charged with 4-nitrophenyl 4-hydroxybenzoate (1 eqv.), the appropriate carboxylic acid (1.5 eqv), EDC.HCl (1.5 eqv.) and DMAP (2 mol%). Dichloromethane was added (conc. ~ 0.1 M) and the suspension stirred until complete consumption of the phenol as judged by TLC. The volatiles were removed in vacuo and the crude material was subjected to flash chromatography over silica gel with a gradient of hexane/DCM. The materials were subsequently recrystallized from EtOH before being dried under reduced pressure to give the reported yields. The quantities and masses of the reagents used are given in SITable 1.

SITable 1: Quantities and masses of the reagents used in the synthesis of Compounds **1-11**.

Compound	Benzoic acid used	Quantity of benzoic acid		Quantity of 4-nitrophenyl 4-hydroxybenzoate		Quantity of EDC.HCl		Quantity of DMAP	
		mg	mmol	mg	mmol	mg	mmol	mg	mmol
1	2,4,6-Trimethoxybenzoic acid	123	0.58	100	0.38	111	0.58	0.9	0.01
2	2-Methoxybenzoic Acid	88	0.58	100	0.38	111	0.58	0.9	0.01
3	2-Methoxy-4-methylbenzoic acid	96	0.58	100	0.38	111	0.58	0.9	0.01
4	2,4-Dimethylbenzoic acid	87	0.58	100	0.38	111	0.58	0.9	0.01
5	2,4,6-Trimethylbenzoic acid	95	0.58	100	0.38	111	0.58	0.9	0.01
6	4-Iodo-2-methoxybenzoic acid	161	0.58	100	0.38	111	0.58	0.9	0.01
7	4-Bromo-2-methoxybenzoic acid	134	0.58	100	0.38	111	0.58	0.9	0.01
8	4-Chloro-2-methoxybenzoic acid	108	0.58	100	0.38	111	0.58	0.9	0.01
9	4-Fluoro-2-methoxybenzoic acid	99	0.58	100	0.38	111	0.58	0.9	0.01
10	3-(2,4-Dimethoxyphenyl)acrylic acid	121	0.58	100	0.38	111	0.58	0.9	0.01
11	5-ethoxy-2-furoic acid	45	0.29	50	0.19	56	0.29	0.5	0.01

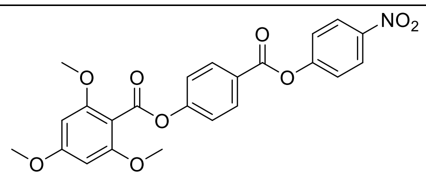

Compound **1**

Appearance	White needles	135 mg, 78 %	
Melting Point	181.9 °C	R_f (DCM:Hex [7:3])	0.19
^{1}H NMR (400 MHz, $CDCl_3$) (δ)	8.34 (d, J = 9.0 Hz, 2H, Ar-**H**), 8.25 (d, J = 8.8 Hz, 2H, Ar-**H**), 7.46 – 7.39 (m, 6H, Ar-**H**), 3.89 (s, 6H, 2x Ar-O-C**H₃** (positions 2 & 6), 3.86 (s, 3H, Ar-O-C**H₃** (position 4)).		
^{13}C{^{1}H} NMR (101 MHz, $CDCl_3$) (δ)	168.51, 164.58, 163.01, 162.11, 156.08, 155.90, 155.04, 145.47, 131.95, 125.87, 125.82, 125.31, 122.67, 122.43, 104.42, 56.15, 55.55		

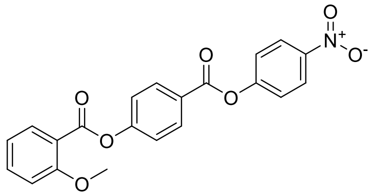

Compound **2**

Appearance	White powder	105 mg, 88 %	
Melting Point	136.4 °C	R_f (DCM:Hex [7:3])	0.58
^{1}H NMR (400 MHz, $CDCl_3$) (δ)	10.53 (s, 1H, Ar-**H**), 8.35 (d J = 9.1 Hz, 2H, Ar-**H**), 8.30 (d, J = 8.8 Hz, 2H, Ar-**H**), 7.98 (d, J = 8.8 Hz, 1H, Ar-**H**), 7.48 – 7.35 (m, 4H, Ar-**H**), 6.61 – 6.49 (m, 2H, Ar-**H**), 3.88 (s, 3H, Ar-O-C**H$_3$**).		
^{13}C{^{1}H} NMR (101 MHz, $CDCl_3$) (δ)	163.59, 163.49, 160.22, 155.80, 155.68, 145.48, 134.93, 132.39, 131.97, 125.85, 125.32, 122.67, 122.44, 120.32, 118.20, 112.30, 56.09.		

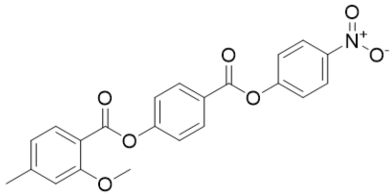

Compound **3**

Appearance	White Powder	108 mg, 70 %	
Melting Point	157.3 °C	R_f (DCM:Hex [7:3])	0.18
^{1}H NMR (400 MHz, $CDCl_3$) (δ)	8.34 (d, J = 9.2 Hz, 2H, Ar-**H**), 8.26 (dd, J = 8.8 Hz, 2H, Ar-**H**), 7.98 (d, J = 7.8 Hz, 1H, Ar-**H**), 7.46 – 7.37 (m, 4H, Ar-**H**), 6.92 – 6.83 (m, 2H, Ar-**H**), 3.95 (s, 3H, Ar-O-C**H$_3$**), 2.45 (s, 3H, Ar-C**H$_3$**).		
^{13}C{^{1}H} NMR (101 MHz, $CDCl_3$) (δ)	163.62, 163.31, 160.49, 155.92, 155.70, 146.36, 145.47, 132.54, 131.92, 125.70, 125.31, 122.67, 122.49, 121.19, 115.12, 113.01, 56.02, 22.15.		

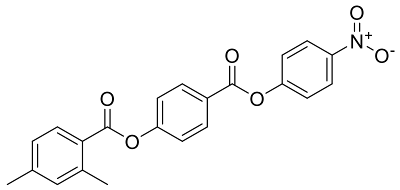

Compound **4**

Appearance	White powder	107 mg, 72 %	
Melting Point	151.1 °C	R_f (DCM:Hex [7:3])	0.48
^{1}H NMR (400 MHz, $CDCl_3$) (δ)	8.34 (d, J = 9.0 Hz, 2H, Ar-**H**), 8.28 (dd, J = 8.8 Hz, 2H, Ar-**H**), 8.10 (d, J = 8.4 Hz, 1H, Ar-**H**), 7.42 (m, 4H, Ar-**H**), 7.20 – 7.11 (m, 2H, Ar-**H**), 2.66 (s, 3H, Ar-C**H**$_3$ (position 2), 2.42 (s, 3H, Ar-C**H**$_3$ (position 4)).		
^{13}C{^{1}H} NMR (101 MHz, $CDCl_3$) (δ)	165.44, 163.57, 155.84, 155.67, 145.49, 144.11, 141.96, 132.98, 132.02, 131.53, 126.83, 125.86, 125.32, 124.81, 122.66, 122.48, 22.03, 21.56.		

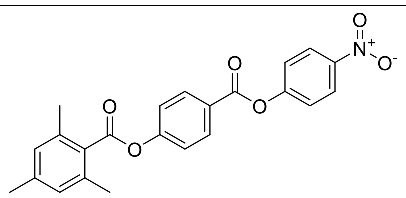

Compound **5**

Appearance	White powder	120 mg, 78 %	
Melting Point	137.8 °C	R_f (DCM:Hex [7:3])	0.39
^{1}H NMR (400 MHz, $CDCl_3$) (δ)	8.34 (d, J = 9.1 Hz, 2H, Ar-**H**), 8.29 (dd, J = 8.7 Hz, 2H, Ar-**H**), 7.50 – 7.38 (m, 4H, Ar-**H**), 6.95 (m, 2H, Ar-**H**), 2.47 (s, 6H, 2x Ar-C**H**$_3$ (positions 2 & 6)), 2.34 (s, 3H Ar-C**H**$_3$ (positions 4)).		
^{13}C{^{1}H} NMR (101 MHz, $CDCl_3$) (δ)	167.61, 163.47, 155.62, 155.46, 145.51, 140.56, 135.91, 132.14, 129.15, 128.87, 126.15, 125.33, 122.66, 122.15, 21.24, 20.16.		

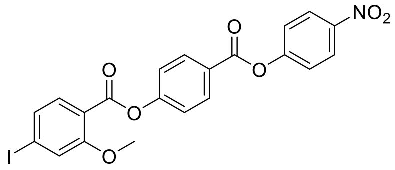

Compound **6**

Appearance	White powder	158 mg, 81 %	
Melting Point	187.7 °C	R_f (DCM:Hex [7:3])	0.34
^{1}H NMR (400 MHz, $CDCl_3$) (δ)	8.34 (d J = 9.2 Hz, 2H, Ar-**H**), 8.30 – 8.24 (m, 2H, Ar-**H**), 7.74 (d, J = 8.2 Hz, 1H, Ar-**H**), 7.46 – 7.37 (m, 6H, Ar-**H**), 3.96 (s, 3H, Ar-O-C**H₃**).		
^{13}C{^{1}H} NMR (101 MHz, $CDCl_3$) (δ)	163.53, 163.01, 160.12, 155.65, 155.55, 145.50, 133.30, 132.00, 129.79, 126.01, 125.33, 122.65, 122.35, 121.97, 117.77, 101.86, 56.43.		

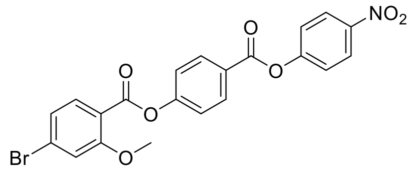

Compound **7**

Appearance	White powder	133 mg, 74 %	
Melting Point	180.0 °C	R_f (DCM:Hex [7:3])	0.28
^{1}H NMR (400 MHz, $CDCl_3$) (δ)	8.34 (d J = 9.2 Hz, 2H, Ar-**H**), 8.27 (d, J = 8.9 Hz, 2H, Ar-**H**), 7.93 (d, J = 8.8 Hz, 1H, Ar-**H**), 7.42 (m, 4H, Ar-**H**), 7.25 – 7.21 (m, 2H, Ar-**H**), 3.97 (s, 3H, Ar-O-C**H₃**).		
^{13}C{^{1}H} NMR (101 MHz, $CDCl_3$) (δ)	163.53, 162.80, 160.63, 155.65, 155.55, 145.50, 133.51, 132.00, 129.41, 126.01, 125.33, 123.68, 122.65, 122.35, 117.10, 116.01, 56.44.		

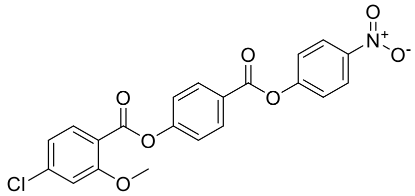

Compound **8**

Appearance	White powder	135 mg, 83 %	
Melting Point	173.6 °C	R_f (DCM:Hex [7:3])	0.22
^{1}H NMR (400 MHz, $CDCl_3$) (δ)	8.33 (d J = 9.1 Hz, 2H, Ar-**H**), 8.27 (d, J = 8.8 Hz, 2H, Ar-**H**), 8.04 – 7.98 (m, 1H, Ar-**H**), 7.46 – 7.36 (m, 4H, Ar-**H**), 7.10 – 7.02 (m, 2H, Ar-H), 3.96 (s, 3H, Ar-O-C**H₃**).		
$^{13}C\{^{1}H\}$ NMR (101 MHz, $CDCl_3$) (δ)	163.52, 162.66, 160.83, 155.65, 155.57, 145.49, 141.02, 133.50, 131.99, 125.99, 125.32, 122.65, 122.37, 120.68, 116.62, 113.04, 56.41.		

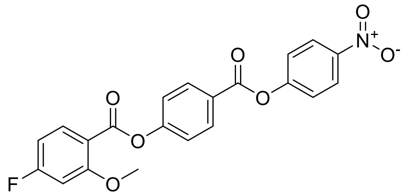

Compound **9**

Appearance	White powder	106 mg, 68 %	
Melting Point	172.0 °C	R_f (DCM:Hex [7:3])	0.39
^{1}H NMR (400 MHz, $CDCl_3$) (δ)	8.33 (d J = 9.2 Hz, 2H, Ar-**H**), 8.27 (dd, J = 8.9 Hz, 2H, Ar-**H**), 8.15 – 8.08 (m, 1H, Ar-**H**), 7.47 – 7.37 (m, 4H, Ar-**H**), 6.82 – 6.73 (m, 2H, Ar-**H**), 3.96 (s, 3H, Ar-O-C**H₃**).		
$^{13}C\{^{1}H\}$ NMR (101 MHz, $CDCl_3$) (δ)	168.26, 165.73, 163.55, 162.51 (d, J = 2.9 Hz), 155.65, 145.48, 134.74, 131.98, 125.92, 125.32, 122.66, 122.41, 114.28 (d, J = 2.9 Hz), 107.59, 100.53, 100.28, 56.40.		
^{19}F NMR (376 MHz, $CDCl_3$) (δ)	100.97 (m, 1F, Ar-**F**).		

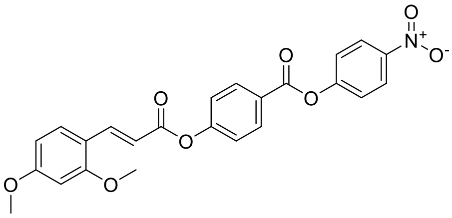

Compound **10**

Appearance	White powder	147 mg, 86 %	
Melting Point	173.2 °C	R_f (DCM:Hex [7:3])	0.53
^{1}H NMR (400 MHz, $CDCl_3$) (δ)	8.33 (d, J = 9.2 Hz, 2H, Ar-**H**), 8.25 (d, J = 9.0 Hz, 2H, Ar-**H**), 8.12 (d, J = 16.0 Hz, 1H, Ar-CH=C**H**-COO), 7.51 (d, J = 8.5 Hz, 1H, Ar-**H**), 7.42 (d, J = 9.2 Hz, 2H, Ar-**H**), 7.36 (d, J = 8.8 Hz, 2H, Ar-**H**), 6.64 (d, J = 16.0 Hz, 1H, Ar-C**H**=CH-COO), 6.58 – 6.52 (m, 1H, Ar-**H**), 6.49 (d, J = 2.4 Hz, 1H, Ar-**H**), 3.91 (s, 3H, Ar-O-C$\mathbf{H_3}$ (position 2)), 3.87 (s, 3H, Ar-O-C$\mathbf{H_3}$ (position 4)).		
^{13}C{^{1}H} NMR (101 MHz, $CDCl_3$) (δ)	165.63, 163.60, 163.43, 160.35, 155.95, 155.71, 145.45, 143.12, 131.94, 131.21, 125.58, 125.30, 122.66, 122.29, 116.17, 114.16, 105.53, 98.49, 55.56.		

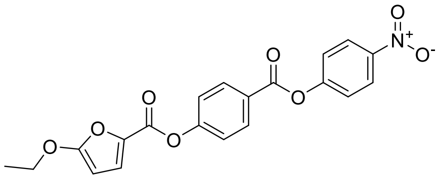

Compound **11**

Appearance	White platelets	100 mg, 66 %	
Melting Point	191.4 °C	R_f (DCM:Hex [7:3])	0.48
^{1}H NMR (400 MHz, $CDCl_3$) (δ)	8.34 (d, J = 9.1 Hz, 2H, Ar-**H**), 8.25 (d, J = 8.9 Hz, 2H, Ar-**H**), 7.46 – 7.35 (m, 6H. Ar-**H**), 5.45 (d, J = 3.7 Hz, 2H, Furan Ar-**H**), 4.29 (q, J = 7.1 Hz, 3H, Furan Ar-O-C$\mathbf{H_2}$-CH_3), 1.48 (t, J = 7.1 Hz, 3H Furan Ar-O-CH_2-C$\mathbf{H_3}$).		
^{13}C{^{1}H} NMR (101 MHz, $CDCl_3$) (δ)	163.53, 163.23, 155.66, 155.24, 149.07, 145.01, 133.05, 132.00, 125.83, 125.32, 124.34, 122.65, 122.19, 85.00, 67.51, 14.49.		

4 References

[1] M. J. and K. C. and H. B. and L. E. Páll Szilárd and Abraham, *Tackling Exascale Software Challenges in Molecular Dynamics Simulations with GROMACS*, in *Solving Software Challenges for Exascale*, edited by E. Markidis Stefano and Laure (Springer International Publishing, Cham, 2015), pp. 3–27.

[2] M. J. Abraham, T. Murtola, R. Schulz, S. Páll, J. C. Smith, B. Hess, and E. Lindah, *Gromacs: High Performance Molecular Simulations through Multi-Level Parallelism from Laptops to Supercomputers*, SoftwareX **1–2**, 19 (2015).

[3] S. Pronk et al., *GROMACS 4.5: A High-Throughput and Highly Parallel Open Source Molecular Simulation Toolkit*, Bioinformatics **29**, 845 (2013).

[4] B. Hess, C. Kutzner, D. Van Der Spoel, and E. Lindahl, *GRGMACS 4: Algorithms for Highly Efficient, Load-Balanced, and Scalable Molecular Simulation*, J Chem Theory Comput **4**, 435 (2008).

[5] D. Van Der Spoel, E. Lindahl, B. Hess, G. Groenhof, A. E. Mark, and H. J. C. Berendsen, *GROMACS: Fast, Flexible, and Free*, J Comput Chem **26**, 1701 (2005).

[6] E. Lindahl, B. Hess, and D. van der Spoel, *GROMACS 3.0: A Package for Molecular Simulation and Trajectory Analysis*, J Mol Model **7**, 306 (2001).

[7] H. J. C. Berendsen, D. Van Der Spoel, and R. Van Drunen, *GROMACS: A Message-Passing Parallel Molecular Dynamics Implementation PROGRAM SUMMARY Title of Program: GROMACS Version 1.0*, Comput Phys Commun **91**, 43 (1995).

[8] J. Wang, R. M. Wolf, J. W. Caldwell, P. A. Kollman, and D. A. Case, *Development and Testing of a General Amber Force Field*, J Comput Chem **25**, 1157 (2004).

[9] C. I. Bayly, P. Cieplak, W. D. Cornell, and P. A. Kollman, *A Well-Behaved Electrostatic Potential Based Method Using Charge Restraints for Deriving Atomic Charges: The RESP Model*, J. Phys. Chem **97**, 10269 (1993).

[10] C. Lee, eitao Yang, and R. G. Parr, *Development of the Colic-Salvetti Correlation-Energy Formula into a Functional of the Electron Density*, Phys Rev B **37**, 15 (1988).

[11] A. D. Becke, *Density-Functional Thermochemistry. III. The Role of Exact Exchange*, Journal of Chemical Physics **98**, 5648 (1993).

[12] M.J.Frisch, G.W.Trucks, H.B.Schlegel, G.E.Scuseria, M.A.Robb, J. R. Cheeseman, G. Scalmani, V. Barone, B. Mennucci, G. A. Petersson, H. Nakatsuji, M. Caricato, X. Li, H. P. Hratchian, A.F.Izmaylov, J.Bloino, G.Zheng, J.L.Sonnenberg, M.Hada, M. Ehara, K. Toyota, R. Fukuda, J. Hasegawa, M. Ishida, T.Nakajima, Y.Honda,O.Kitao, H.Nakai,T.Vreven, J. A. Montgomery Jr., J. E. Peralta, F. Ogliaro, M. J. Bearpark, J.Heyd, E.N.Brothers, K.N.Kudin, V.N.Staroverov,R. Kobayashi, J. Normand, K. Raghavachari, A. P. Rendell, J.C.Burant, S.S.Iyengar, J.Tomasi, M.Cossi, N.Rega,N.J.Millam, M.Klene, J.E.Knox, J.B.Cross, V.Bakken, C.Adamo, J. Jaramillo, R. Gomperts, R. E. Stratmann, O. Yazyev, A. J. Austin,R. Cammi, C. Pomelli, J. W. Ochterski, R. L. Martin, K.Morokuma, V.G.Zakrzewski, G.A.Voth, P.Salvador, J.J.Dannenberg, S. Dapprich, A. D. Daniels, O ̈.Farkas,J.B.Foresman ,J.V.Ortiz, J.CioslowskiandD.J.Fox, Gaussian 09, Revision E.01, Gaussian, Inc., Wallingford CT, 2009.

[13] J. Wang, W. Wang, P. A. Kollman, and D. A. Case, *Automatic Atom Type and Bond Type Perception in Molecular Mechanical Calculations*, J Mol Graph Model **25**, 247 (2006).

[14] D. A. Case, T. E. Cheatham, T. Darden, H. Gohlke, R. Luo, K. M. Merz, A. Onufriev, C. Simmerling, B. Wang, and R. J. Woods, *The Amber Biomolecular Simulation Programs*, J Comput Chem **26**, 1668 (2005).

[15] D. Silva and B. F. Vranken, *ACPYPE-AnteChamber PYthon Parser InterfacE*, Research Notes **5**, 367 (2012).

[16] B. Hess, H. Bekker, H. J. C. Berendsen, and J. G. E. M. Fraaije, *LINCS: A Linear Constraint Solver for Molecular Simulations*, J Comput Chem **18**, 1463 (1997).

[17] S. Nosé and M. L. Klein, *Constant Pressure Molecular Dynamics for Molecular Systems*, Mol Phys **50**, 1055 (1983).

[18] M. Parrinello and A. Rahman, *Polymorphic Transitions in Single Crystals: A New Molecular Dynamics Method*, J Appl Phys **52**, 7182 (1981).

[19] W. G. Hoover, *Canonical Dynamics: Equilibrium Phase-Space Distributions*, Phys Rev A (Coll Park) **31**, 1695 (1985).

[20] S. Nosé, *A Molecular Dynamics Method for Simulations in the Canonical Ensemble*, Mol Phys **52**, 255 (1984).

[21] R. T. McGibbon, K. A. Beauchamp, M. P. Harrigan, C. Klein, J. M. Swails, C. X. Hernández, C. R. Schwantes, L. P. Wang, T. J. Lane, and V. S. Pande, *MDTraj: A Modern Open Library for the Analysis of Molecular Dynamics Trajectories*, Biophys J **109**, 1528 (2015).

[22] R. J. Mandle, *Implementation of a Cylindrical Distribution Function for the Analysis of Anisotropic Molecular Dynamics Simulations*, PLoS One **17**, (2022).